Light-induced adaptive laboratory evolution enhances bioactive aromatic amino acid-derived compound profile in a wine strain of Saccharomyces

Food Microbiology 142 (2027) 105295

Contents lists available at ScienceDirect

Food Microbiology

journal homepage: www.elsevier.com/locate/fm

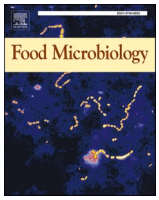

Light-induced adaptive laboratory evolution enhances bioactive aromatic amino acid-derived compound profile in a wine strain of *Saccharomyces cerevisiae*

Ricardo Bisquert [a,b], Alba Guillén [a], Guillermo Quintas [c], José M. Guillamón [a,*]

[a] Institute of Agrochemistry and Food Technology, Department of Food Biotechnology (IATA-CSIC), Avda. Agustín Escardino, 7, Paterna, 46980, Spain
[b] Department of Life Sciences, Chalmers University of Technology, Kemivägen 10, Gothenburg, SE-412 96, Sweden
[c] Health and Biomedicine, Leitat Technological Center, Baldiri Reixac 15, Barcelona, 08028, Spain

ARTICLE INFO

Keywords:
Wine yeast
Adaptive evolution
Bioactive metabolites
Transcriptomics
Metabolomics

ABSTRACT

Yeast metabolism plays a key role in the synthesis of bioactive compounds in fermented foods and beverages. Among these, aromatic amino acid-derived compounds (AADCs) such as tryptophol, 2-phenylethanol, and tyrosol, along with indolic compounds like melatonin, serotonin, and 3-indoleacetic acid, contribute to the quality and stability of wine. This study aimed to enhance the production of these compounds in *Saccharomyces cerevisiae* through adaptive laboratory evolution (ALE) using white light as a selective pressure. The hypothesis was that oxidative stress induced by light would stimulate non-enzymatic antioxidant responses, increasing the synthesis of indolic compounds. A wine yeast strain was subjected to ALE, and the evolved strain was analyzed for genotypic, phenotypic, and metabolomic changes. Results showed significant genomic and transcriptomic differences, leading to a marked increase in AADC production. These findings highlight this approach as a promising non-GMO strategy for improving yeast strains in the food industry.

1. Introduction

The presence of bioactive molecules in fermented foods and beverages is closely associated with microbial metabolism, with yeasts standing out as major contributors to the synthesis of these health-promoting compounds (Marhuenda et al., 2016; Rodriguez-Naranjo et al., 2011; Vilela, 2019). Among them, aromatic amino acid-derived compounds (AADCs), such as tryptophol (TOL), 2-phenylethanol (2 PE), and tyrosol, as well as indolic compounds derived from tryptophan (Trp), including melatonin (Mel), serotonin, and 3-indoleacetic acid (3IAA), are particularly relevant because they contribute to the quality and stability of fermented beverages such as wine (Cordente et al., 2019; Fernández-Cruz et al., 2016). In this context, the development of yeast strains capable of increasing the concentration of these compounds in the final product is of great interest to the wine and other food industries. The antioxidant, antimicrobial, preservative, and health-promoting properties associated with the presence of bioactive AADCs, are highly valued in fermented products. To this end, we recently designed a consortium of different *Saccharomyces* species that significantly enhances the content of bioactive tryptophan-derived compounds during wine fermentation (Planells-Cárcel et al., 2024).

An alternative to the selection of naturally high AADC-producing yeast strains is their genetic improvement for use in beverage production. However, the generation of yeast strains with these desirable traits faces two major challenges. First, the effective and precise metabolic engineering of yeast to increase the production of a specific metabolite requires a comprehensive understanding of its biosynthetic pathway, including the involved precursors, cofactors, genes, enzymes, synthesis conditions, as well as potential bottlenecks and metabolic leakage points. Although significant progress has been made in recent years in elucidating AADC metabolism (Muñiz-Calvo et al., 2019; Planells-Cárcel et al., 2025), key aspects remain unresolved for some of the most bioactive and industrially relevant compounds, such as melatonin, serotonin, and hydroxytyrosol (HT), in yeast. Secondly, even when detailed knowledge of the biosynthetic process is available, the rational design of yeast strains for use in the food industry is severely restricted by European legislation, particularly Regulation (EC) No 1829/2003 concerning genetically modified organisms (GMOs).

The quest for genetically improving industrial yeast strains without the commercial and regulatory constraints of being considered a GMO

* Corresponding author.
E-mail address: guillamon@iata.csic.es (J.M. Guillamón).

https://doi.org/10.1016/j.fm.2026.105295
Received 6 May 2026; Received in revised form 26 August 2026; Accepted 29 August 2026
Available online 2 September 2026

gave rise to a series of methods to achieve genetic diversity to get to the desired phenotypical traits. These approaches include random mutagenesis, intra- and interspecific hybridization and adaptive laboratory evolution (ALE), also referred as directed evolution (Gonzalez and Morales, 2022). Among them, ALE has been successfully conducted to improve yeast tolerance to freeze-thaw, salt, acetic acid, temperature and ethanol in industrial yeast strains (Aarnio et al., 1991; García-Ríos et al., 2022; Matsutani et al., 1992; Novo et al., 2014; Takagi et al., 1997). This approach is based on the natural genetic and phenotypic diversity of yeast, that is iteratively subjected to a selective pressure through multiple generations that allows population to fix genetic and phenotypic traits that are different from the initial parental strain. When improving traits such as ethanol tolerance and the others above mentioned, a relatively straight-forward experimental design is often used, but in some cases indirect selection strategies are needed, *e.g.* the use of a selective pressure such as osmotic stress to select strains with higher glycerol production (Tilloy & Ortiz-julien, 2014). In this work a novel directed evolution experiment was conducted using a *Saccharomyces cerevisiae* strain, isolated from a winery environment, and employing a very particular selective pressure, such as white light.

It has been reported that visible light exerts a significant impact on yeast metabolism by damaging cytochromes and promoting the generation of reactive oxygen species (ROS), thereby triggering an oxidative stress response (Robertson et al., 2013). This response is initiated by a peroxisomal oxidase that converts light exposure into a hydrogen peroxide (H_2O_2) signal. The signal is sensed by the peroxiredoxin Tsa1 and subsequently relayed to thioredoxin (Bodvard et al., 2017). Furthermore, although direct evidence of white light-induced mutagenesis in yeast remains limited, early studies by Webb & Malina (1967) demonstrated that visible light increased mutation rates in *Escherichia coli* to levels more than 18-fold higher than spontaneous rates, with mutation frequency positively correlated with irradiance. Bioactive AADCs such as HT and especially Trp-derived ones such as serotonin, tryptamine and Mel, among others, have an antioxidant effect on yeast at different levels, acting as free-radical scavengers but also by inducing expression of oxidative response genes (Bisquert et al., 2018; Vázquez et al., 2017). Taking Mel as a model of a potent antioxidant indolic compound and its relation to light stimuli in higher organisms and its UV protection effect in yeast cells (Bisquert et al., 2018), a physical ROS-generating selective pressure, such as white light, was employed in an ALE experiment. The proposed hypothesis was that the primary responses of cells to oxidative stress would be challenged in a directed evolution context when generating a photooxidation by illuminating the growth vessel with a white light LED lamp, which covered mainly photosynthetically active radiation (PAR) wavelengths ranging from 400 to 700 nm. Among these primary oxidative stress defense systems, the increase of non-enzymatic forms of antioxidant response such as the synthesis of melatonin or other indolic and phenolic compounds was therefore a possible and expectable outcome.

In this study, a commercial wine yeast strain was subjected to adaptive laboratory evolution (ALE) using white light as a selective pressure during successive batch cultures. In parallel, the same strain was cultivated under identical conditions in the absence of white light, serving as a control. Genotypic and phenotypic differences between the light-evolved and control strains were systematically evaluated. To this end, comparative analyses of whole-genome sequences, intracellular and extracellular metabolomic profiles, and transcriptomic responses were performed. This comprehensive analysis established extensive genomic modifications as an adaptive advantage against white light and described the interesting co-occurrence of the relative increased production of bioactive AADCs in the evolved strain, altered transcriptional activity involving AADCs pathways and specific point mutations in involved genes. Furthermore, the potential of white light as a severe selective pressure, and even as a mutagen to be used in future developments of new strains from a non-GMO approach was revealed.

2. Materials and methods

2.1. Yeast and growth media

A *Saccharomyces cerevisiae* strain was first isolated in 2019 from a winery fermentation tank (Bodegas Murviedro; Requena, SPAIN) at the end of an industrial fermentation of "Bobal" grapes must, genotyped using mitochondrial DNA, as described in Querol et al. (1992), and codified as B28. For preculture growth, yeast extract peptone dextrose (YPD) medium containing yeast extract 10 g L^{-1}, bacteriological peptone 20 g L^{-1} and glucose g·L^{-1} was used. A synthetic minimal media (SMM) was employed for the evolution experiment, containing 7.5 g L^{-1} glucose, 5 g L^{-1} $(NH_4)_2SO_4$, 3 g L^{-1} KH_2PO_4, 0.5 g L^{-1} $MgSO_4$, 1 mL L^{-1} vitamins solution, 1 mL L^{-1} oligo-elements solution, and pH was adjusted to 6 with NaOH. Vitamins solution contained 2 g L^{-1} myo-inositol, 0.15 g L^{-1} calcium pantothenate, 0.025 g L^{-1} thiamine hydrochloride, 0.2 g L^{-1} nicotinic acid, 0.025 g L^{-1} pyridoxine and 0.3 mg L^{-1} biotin. Oligo-elements solution contained 4 g L^{-1} $MnSO_4 \cdot H_2O$, 4 g L^{-1} $ZnSO_4 \cdot 7\ H_2O$, 1 g L^{-1} $CuSO_4 \cdot 5\ H_2O$, 1 g L^{-1} KI, 0.4 g L^{-1} $CoCl_2 \cdot 6\ H_2O$, 1 g L^{-1} H_3BO_3 and 1 g L^{-1} $(NH_4)_6Mo_7O_{24}$.

Growth assays using 96-well plates were performed using SD (20 g L^{-1} glucose, 1.7 g L^{-1} yeast nitrogen base (YNB) without amino acids and $(NH_4)_2SO_4$ (Difco) and 5 g L^{-1} $(NH_4)_2SO_4$), SC (20 g L^{-1} glucose, 1.7 g L^{-1} yeast nitrogen base (YNB) without amino acids and $(NH_4)_2SO_4$ (Difco), 5 g L^{-1} $(NH_4)_2SO_4$ and 2 g L^{-1} SC complete drop-out (Formedium)), and YPG (10 g L^{-1} yeast extract, 20 g L^{-1} peptone, and 30 mL of glycerol).

Fermenting ability of the evolved and the control strain was assessed using synthetic must (SM) derived from Riou et al. (1989) to mimic a wine fermentation. SM composition consisted of sugars (100 g L^{-1} glucose and 100 g L^{-1} fructose), organic acids (citric acid, malic acid and tartaric acid), mineral salts (0.75 g L^{-1} KH_2PO_4, 0.5 g L^{-1} K_2SO_4, 0.25 g L^{-1} $MgSO_4 \cdot 7\ H_2O$, 0.15 g L^{-1} $CaCl_2 \cdot 2\ H_2O$, 0.20 g L^{-1} NaCl and 0.46 g L^{-1} NH_4Cl), 13.09 mL L^{-1} amino acids from stock (1.5 g L^{-1} tyrosine, 13.4 g L^{-1} Trp, 2.5 g L^{-1} isoleucine, 3.4 g L^{-1} aspartic acid, 9.2 g L^{-1} glutamic acid, 28.3 g L^{-1} arginine, 3.7 g L^{-1} leucine, 5.8 g L^{-1} threonine, 1.4 g L^{-1} glycine, 38.4 g L^{-1} glutamine, 11.2 g L^{-1} alanine, 3.4 g L^{-1} valine, 2.4 g L^{-1} methionine, 2.9 g L^{-1} phenylalanine, 6 g L^{-1} serine, 2.6 g L^{-1} histidine, 1.3 g L^{-1} lysine, 1.5 g L^{-1} cysteine, 46.1 g L^{-1} proline), 10 mL L^{-1} vitamins solution and 1 mL L^{-1} oligo-elements solution. pH was adjusted to 3.3 with NaOH. The control strain (B28 cultivated in absence of light) and its evolved version in presence of light (EVO) were inoculated in 80 mL of SM and grown in fermentation flasks capped with airlock valves, incubated at 28 °C with 200 rpm orbital shaking, and the weight loss was monitored until stabilization.

2.2. Adaptive laboratory evolution under white light stress

B28 strain was subjected to ALE using white light as a selective pressure. The light source was a white LED lamp covering PAR wavelengths from 400 to 700 nm. In parallel, B28 was also cultivated under identical conditions in the absence of white light (hereafter referred as "CONTROL").

Batch cultures were grown at 28 °C in two 0.5 L reactors (MiniBio, Applikon Biotechnology) with a working volume of 0.4 L of SMM media. The culture temperature was controlled using a temperature probe connected to a Peltier cryostat. The stirrer was set at 300 rpm. Both bioreactors were initially inoculated with approximately 2×10^6 cells·mL^{-1} of B28 strain from a preculture previously grown overnight in YPD medium. One of the bioreactors was illuminated with a white JARO led lamp (Brennenstuhl®, Tübingen, Germany) at an initial irradiance of 317 μmol m^{-2}·s^{-1}, positioned 16 cm from the vessel, a distance at which a clear effect on yeast growth was observed. The control bioreactor was set to the same growth conditions except for the light stimulus. The bioreactors were depleted of ~90 % of the spent media and refilled with fresh media when cultures reached the

stationary phase. Optical density measured at 600 nm (OD_{600}) was registered at the beginning and end of each batch to estimate the number of generations (g) according to g = (*log*(finalOD)-*log*(initialOD))/*log*(2). Selective pressure produced a growth defect on the stressed population at the initial dose (317 μmol $m^{-2}{\cdot}s^{-1}$), forcing it to grow at a slower pace than the non-challenged population. The pressure was increased gradually across the different batches, as the cells duplication time shortened due to their adaptation, until irradiance reached 3377 μmol $m^{-2}{\cdot}s^{-1}$, which corresponded to a distance of 4 cm from the vessel, while still allowing cell growth. After approximately 170 generations the evolution experiment was concluded. Cells from both vessels were collected, plated and three independent colonies per vessel were grown and glycerinated. One colony from each vessel was selected for whole-genome sequencing. For transcriptomic and metabolomic analyses, three independent colonies from each vessel were used, representing independent derivatives of the evolved and control populations, respectively.

2.3. Growth curve analysis

All the presented growth curves were obtained from growth on 96-well microtiter plates. Each well was filled with 250 μL of the different media and condition and an initial OD_{600} of 0.1 was used to inoculate them from previously grown overnight precultures. Growth curves were monitored by recording the increase of the OD_{600}. The microtiter plates were incubated in SPECTROstar Nano® microplate reader (BGM Labtech, Offenburg, Germany) at 28, 20 or 12 °C with 500 rpm double-orbital shaking. The OD_{600} of each well was measured every 30 min until the growth reached the stationary phase. The growth parameters of each strain under different media/condition can be calculated by directly fitting OD_{600} measurements versus time to the Gompertz equation proposed by Zwietering et al. (1990), which has the following expression:

$$y = D \times e^{-e\left(\frac{\mu_{max} \times e}{D}\right) \times (\lambda - t) + 1}$$

Where $y = \ln(OD_t/OD_0)$, OD_0 is the initial OD and OD_t is the OD at time t; $D = \ln(OD\infty/OD_0)$ is the OD value reached with OD∞ as the asymptotic maximum, μmax is the maximum specific growth rate (h^{-1}), and λ is the lag phase period. *R* software (v4.1.3) was used to fit growth data to Gompertz equation and infer growth parameters.

The area under the curve (AUC), which represents the three main growth parameters: lag phase, μ_{max} and maximum population (yield), was calculated using Origin Pro 2019.

2.4. Intracellular reactive oxygen species (ROS) measuring by flow cytometry

After an overnight growth in a rich YPD medium, the intracellular ROS levels of the freshly inoculated yeast cells were measured as described in Ballester-Tomás et al. (2015). Briefly, grown cell cultures of both CONTROL and EVO strains were centrifuged and resuspended to OD_{600} = 0.25 in sterile PBS. Then dihydrorhodamine 123 (DHR 123, Sigma) was added at 5 μg mL^{-1} of cell culture from a 2.5 mg mL^{-1} stock solution in ethanol. Cells were incubated in darkness for 90 min at 28 °C. Then cells were collected, washed, resuspended in PBS and analyzed using a flow cytometer MACSQuant® Analyzer (Miltenyi Biotec, Madrid, Spain). The settings were adjusted using negative (DHR 123-untreated cells) and positive (stressed with 4 mmol L^{-1} H_2O_2 for 60 min and DHR 123-stained cells) controls. Data were expressed as the percentage of cells that show DHR 123-positive staining where 10000 cells were measured in each run.

2.5. Genomic DNA extraction

Yeast genomic DNA was extracted from 1 to 5 mL cultures grown normally in YPD according to the method described in Querol et al. (1992). Briefly, cells from grown precultures were pelleted and washed twice with sterile water, then resuspended in 0.5 mL of Buffer 1 (0.9 mol L^{-1} sorbitol, 0.1 mol L^{-1} EDTA pH 7.5) and 30 μL of Zimolyase (amsbio) were added for a mild mixing and incubation at 37 °C for 30 min. Spheroplasts were centrifuged 3 min at 15000 × g and resuspended in Buffer 2 (50 mM Tris pH 7.4, 20 mM EDTA). Then 13 μL of 100 g L^{-1} SDS were added and incubated during 5 min at 65 °C. After incubation, 200 μL of 5 mol L^{-1} potassium acetate were added, mildly mixed by inversion and kept on ice for 10 min. After this, tubes were centrifuged at 4 °C for 15 min at 15000 × g to remove the SDS by precipitation. The supernatants were transferred to new tubes and 0.7 mL of isopropanol were added prior to a brief 10 min incubation at room temperature. After incubation, tubes were centrifuged at 4 °C for 15 min at 15000 × g and supernatants were discarded. Pellets were then washed with 0.5 mL of 70 % ethanol. After centrifugation for 3 min 15000 × g supernatants were eliminated and pellets were dried under vacuum and re-suspended in TE (10 mmol L^{-1} Tris, 1 mmol L^{-1} EDTA, pH 8.0) or Milli-Q water.

2.6. Genome sequencing and analysis of the parental and evolved strain

The CONTROL strain and the evolved strain EVO, were sequenced. DNA Libraries were generated using Illumina Truseq Nano DNA library Preparation following manufacturer's recommendations. Libraries were sequenced on an MiSeq instrument and 15M 2 × 250 pb pair-end reads generated. Raw sequencing reads in FASTQ format were subjected to initial quality control and preprocessing. First, fastp v0.23.2 (Chen et al., 2018) was used for adapter removal and filtering of low-quality reads. Processed data quality was then assessed using FastQC v0.11.9 (Andrews, 2010), generating individual quality reports.

All sequence samples were aligned against reference strain genome S288C with bowtie2, and deletions and insertions were assessed with CNVnator. Sequencing reads from each strain were mapped against the reference assembly of the original strain. Variant calling was performed using Breseq, to identify sequence changes based on these alignments. Subsequently, gdtools was used to annotate the detected mutations, determining whether they occur in intergenic or coding regions, identifying the affected gene, and predicting the impact on the coding sequence.

Additionally, all mutations were compared across the different strains using gdtools, to identify mutations unique to specific evolved strains. This comparative approach allowed for the filtering of heterozygous mutations already present in the ancestral strain. This enabled the distinction between pre-existing heterozygosity and mutations that emerged during the evolution process. A filtered table containing the mutations details was generated (Supplementary material).

2.7. RNA extraction

To study global gene expression under melatonin synthesis conditions, preinocula of CONTROL and EVO were grown overnight in synthetic minimal media (SMM) from three independent colonies of each strain and inoculated in 250 mL shake flasks containing 100 mL of fresh medium (SMM) to an initial OD_{600} of 0.15 and incubated at 28 °C with 150 rpm orbital shaking. Strain EVO was also grown in parallel under light stress, at an irradiance between 2306 and 3077 μmol $m^{-2}{\cdot}s^{-1}$. A total of three different sample groups were generated: CONTROL, EVO and LIGHT (EVO strain grown under light stress). Strain CONTROL did not grow under light conditions. Each sample was centrifuged and cell pellets were frozen using liquid nitrogen and then stored at −80 °C until subsequent RNA extraction and intracellular content preparation for metabolomic analysis. Supernatant was also collected for metabolome

analysis under these experimental conditions.

To extract RNA, cell pellets were resuspended in 0.4 mL of LETS buffer (0.1 mol L^{-1} LiCl, 0.01 mol L^{-1} EDTA, pH 8.0, 0.01 mol L^{-1} Tris-HCl, pH 7.4, and 2 g L^{-1} SDS) and added to 2 mL screw tubes containing 0.4 mL of phenol (pH 4.5)-chloroform (5:1) and 0.3 mL of glass beads. Then cells were ruptured with a Tehtnica MillMix 20 homogenizer (Tehtnica, Slovenia). Supernatants were treated with phenol–chloroform (5:1) and chloroform-isoamyl alcohol (24:1) to extract RNA. RNA was precipitated at −20 °C overnight two times, first by adding 2.5 vol of 96 % ethanol and 0.1 volume of 5 mol L^{-1} LiCl, and secondly by adding 2.5 vol of 96 % ethanol and 0.1 volume of 3 mol L^{-1} sodium acetate. RNA was reconstituted in RNase-free MilliQ water and quantified in a NanoDrop spectrophotometer (Thermo Scientific, United States).

2.8. RNA sequencing (RNAseq)

RNA sequencing was performed by the SCSIE (University of Valencia). Briefly, RNA quality was determined with a Bioanalyzer 2100 (Agilent) and concentration measured with a Qubit®2.0 (Life Technologies, USA), yielding RNA integrity numbers (RIN) between 9.4 and 9.7, thus indicating nearly intact RNA, and concentrations ranged between 400 and 900 ng mL^{-1} across all samples. TruSeq® stranded mRNA Kit (Illumina, USA) was used to prepare the libraries for RNA-Seq following the manufacturer's protocol and they were sequenced on an Illumina HiSeq 2500 with 2×75-bp paired-end reads. Adapters from raw reads were trimmed with *trimmomatic*. *FastQC* was used to assess read quality and adapter content, then reads were mapped using S288c reference genome with *Bowtie2* and counts tables were obtained with *htseq-count*. The gene expression abundance was normalized by log2-CPM (counts per million, corrected for the different library sizes, expressed in a log2 scale) using *edgeR* (v3.36.0). *limma* package (v3.50.3) was used to estimate log2-CPM mean variance, establish the different contrasts of hypothesis and an empirical Bayes moderation of the standard errors was applied to increase statistical power of differentially expressed genes (DEGs). Significance ($p < 0.05$) was accounted on the corrected *p*-value obtained from the tests applied by *eBayes* module (*limma* package). Whole statistical computing was run on R software (v4.1.3).

Enrichment of GO terms and gene clustering was analyzed based on the identified DEGs using STRING v12.0 database (http://www.string-db.org). Specific gene functions and biological pathways were annotated according to SGD (http://www.yeastgenome.org) and UniProt (http://www.uniprot.org).

2.9. Metabolomic analysis

EVO and CONTROL strains were grown in SMM at 28 °C and constant shaking under the same conditions in the dark. In parallel, three more replicates of EVO strain were grown, but challenged with constant white illumination (LIGHT). Lamp was again set to exert 3377 μmol $m^{-2}{\cdot}s^{-1}$ of PAR radiation to the shake flasks for 72 h, CONTROL strain could not grow under these conditions. Supernatants and cells (to a final $OD_{600} = 40$) were collected and pellets were washed twice with deionized water, resuspended in 700 μL of phosphate buffered saline (PBS), and transferred to 2 mL tubes containing 0.3 μL of 0.5 mm glass beads (Sigma Aldrich). Then cells were ruptured by applying three shaking cycles at 30 s^{-1} for 30 s in a Tehtnica MillMix 20 homogenizer (Tehtnica, Slovenia), centrifuged at 10000 × *g* for 10 min and all supernatants were kept at −20 °C until analysis. Samples were thawed at room temperature, vortexed for 15 s and centrifuged at 10000 × *g* for 15 min at 4 °C. 100 μL of samples were placed into 1.5 mL Eppendorf tubes and mixed with 60 μL of H_2O and 60 μL of a HCOOH solution (0.1 % v/v) in CH_3CN. Samples were mixed (vortex, 15 s) and transferred to a 96-well plate for UPLC-MSMS analysis. Sample analysis was carried out in an Agilent 1290 Infinity UPLC chromatograph using a UPLC BEH C18 column (100 × 2.1 mm, 1.7 μm, Waters, Wexford, Ireland). Autosampler and column temperatures were set to 4 and 40 °C, respectively, and the injection volume was 4 μL. Gradient elution was performed at a flow rate of 400 μL min^{-1} as follows: initial conditions of 98 % of mobile phase A (H_2O (0.1 % v/v HCOOH)) were kept for 0.5 min, followed by a linear gradient from 2 to 25 % of mobile phase B (CH_3CN (0.1 % v/v HCOOH)) in 3.0 min and from 25 to 98 % B in 4.5 min. Conditions of 98 % B were held for 1 min; then, a 0.25 min gradient was used to return to the initial conditions, which were held for 2.0 min.

All solvents were of LC-MS grade and were purchased from Scharlau (Barcelona, Spain). Ultrapure water was generated with a Milli-Q water purification system (Merck Millipore, Darmstadt, Germany).

Formic acid (≥95 %) was obtained from Sigma-Aldrich Quimica SA. Full-scan MS data from 100 to 1700 m/z with a scan frequency of 5 Hz were collected on an iFunnel quadrupole time-of-flight (QTOF) Agilent 6550 spectrometer (Agilent Technologies, CA, USA) in the TOF MS mode. The following electrospray ionization parameters were selected in positive and negative modes: gas T, 200 °C; drying gas, 14 L min^{-1}; nebulizer, 35 psig; sheath gas T, 350 °C; sheath gas flow, 11 L min^{-1}. Automated UPLC-ESI(+/−)-QqTOF (MS/MS) analysis of the QC was carried out by data dependent acquisition (DDA) to support compound identification using 20 V as collision energy. Metabolite identification was based on MS (isotopic profile) and MS/MS spectral matching, following the criteria described by Ten-Doménech et al. (2020), including m/z tolerance (30 ppm) and retention time tolerance (0.1 min) between experimental and reference spectra to ensure an accurate annotation. The MS/MS spectral match for metabolites of interest are detailed in Fig. S1. System conditioning and data clean-up was carried out as described in Martínez-Sena et al. (2019).

Peak table generation was carried out using XCMS software. The *centWave* method was used for peak detection with the following parameters: mass accuracy: 20 ppm, peak width: (5,25), snthresh: 12, prefilter: (5,5000). Overlapping peaks were considered as distinct when the minimum difference in *m/z* was 7.5 mDa. *wMean* function was used to calculate the intensity weighted *m/z* values of each feature. Mexican hat-filtered raw data with enhanced peak-shaped features was used to establish peak limits used for integration. Grouping before and after RT correction was carried out using the *nearest* method and 9 s as *rtCheck* argument. Finally, missing data points were filled by reintegrating the raw data files in the regions of the missing peaks using the *fillPeaks* method. XCMS data for each sample and UPLC-MS feature were used to extract the peak area, retention time (RT) and peak widths.

Blank samples were used to perform the data clean-up. Biological samples qualified as "informative" UPLC-MS features when their minimum signal exceeded at least three times the maximum signal from the blanks. Due to the limited number of analyzed samples, QCs were injected at the beginning and end of the sequence, but no within-batch effect correction was required (Sánchez-Illana et al., 2018). Analytical results from extracellular matrix were normalized by cell density.

Samples were additionally analyzed using a targeted quantitative UPLC-MSMS method as described in Lario et al. (2017). Briefly, an Acquity HSS T3 C18 (100 × 2.1 mm, 1.8 μm) column was used with H2O (0.1 % v/v HCOOH) (A) and (0.1 % v/v HCOOH) CH3CN (B) as mobile phases. Gradient elution started with phase B held at 2 % from 0 to 0.5 min followed by a linear increase to 45 % 5 min. Then phase B to 90 % in 0.2 min following a fast return to initial conditions between 5.7 and 6 min. With a column re-equilibration of 1.5 min. Injection volume, flow rate and column temperature were set at 3 μL, 550 μL/min and 55 °C, respectively. Samples were held at 6 °C during analysis. Electrospray ionization was carried out using the following conditions: capillary 2.9 kV, cone 25 V, source temperature 120 °C, desolvation temperature 395 °C, N2 cone and desolvation gas flow rates were 150 and 800 L/h, respectively. The list of quantified analytes and their parameters are detailed in Table S.1.

3. Results and discussion

3.1. Evolution under light-induced stress

A strong resistance against a challenging environment and oxidative stress was expected from the original wine strain due to its origin and the fact that it previously endured an entire industrial fermentation process without being completely displaced across the winemaking process, but it is interesting to note that the growth of B28 was severely affected by light, even at the initial irradiance of 317 μmol $m^{-2}{\cdot}s^{-1}$. Therefore, the radiation was initially applied in intervals of 17 h to allow the cells to partially recover in darkness and eventually reach the stationary phase. After 170 generations, the EVO strain was able to grow under an irradiance 10 times higher than the initial level. This contrasted with the fact that the CONTROL strain, which was cultured for the same number of generations under light-free conditions, was completely unable to grow under these conditions of light exposure. This indicated that the EVO strain would be able to adapt to the strong selective pressure of white light irradiation due to its genetic differences from the CONTROL strain. As a track of the progress across the experiment, the generations occurring in each batch and the radiation dose received in each batch were recorded (Fig. 1). The great effect exerted by this chosen selective pressure underscores its potential as a severe stressor. During the evolution experiment, the level of irradiance was gradually increased to a maximum of 3377 μmol $m^{-2}{\cdot}s^{-1}$ as the growth under the stress condition became similar to that of the non-stressed control, which was growing in parallel in a non-irradiated bioreactor. As observed in early stages of ALE, cells enduring ~70 mol of photons per square meter duplicated three to five times during a batch while in final stages they duplicated four to five times but endured ~290 mol m^{-2} of accumulated radiation (Fig. 1).

3.2. Phenotypic traits resulting from ALE

A clear resistance to white light achieved throughout ALE allowed EVO strain to grow under radiation conditions that are incompatible with cell growth for the parental B28 or for the CONTROL strain. This study aims to further explore phenotypic differential traits, particularly those related to the EVO metabolic profile compared to the CONTROL strain, as well as any other traits affecting growth parameters, oxidative stress resistance and fermentative performance. Light-induced stress is known to produce an increase of intracellular ROS that can affect growth

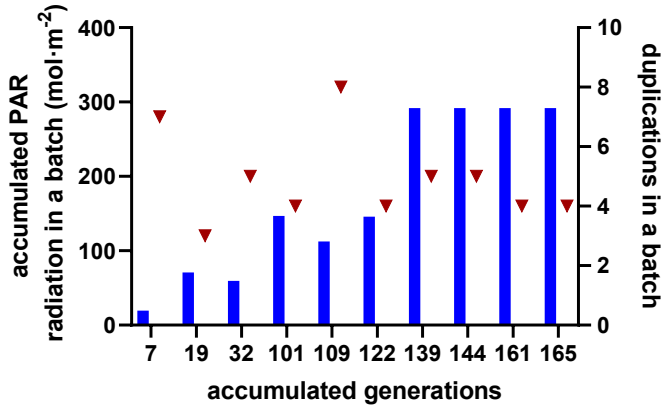

Fig. 1. Evolution process of B28 strain across multiple generations is shown by the number of duplications occurring in a batch (red triangles) in relation to the stress severity, shown as accumulated PAR radiation in the same batch. Irradiance describes the amount of energy received per unit of time. To better reflect the total dose received by the bioreactor, the time of each batch was taken into account when calculating the accumulated photosynthetically active radiation (PAR) (blue bars). (For interpretation of the references to colour in this figure legend, the reader is referred to the Web version of this article.)

but also the expression of genes involved in oxidative stress response (Bodvard et al., 2017; Robertson et al., 2013).

To assess the growth performance under oxidative stress, CONTROL and EVO strains were grown in 96-well plates under different media and conditions. When the strains were grown using the same medium and temperature as those used in the directed evolution batches, EVO strain performed similar to the CONTROL strain, but with a significant delay, as observed in the growth curves (Fig. 2A) and indirectly reflected in the area under the curve (AUC) parameter (Fig. 2C). Contrary to what was expected, an improvement in EVO growth compared to CONTROL was not observed when cells were challenged with 3 mM of hydrogen peroxide to increase oxidative stress (Fig. 2B). In fact, EVO strain showed a greater sensitivity to H_2O_2 and reflected it as a very pronounced delay in growth when compared to the control strain. With the aim of partially delimiting the causes of the slower growth in EVO strain, intracellular ROS levels were measured by determining the abundance of DHR123-positive cells in non-stressed cultures using a flow cytometer. Surprisingly EVO strain exhibited a significantly higher proportion of DHR123-positive cells than CONTROL under the same condition without stress (Fig. 2D). These differences in the default intracellular ROS levels could explain the slower growth for EVO strain, as evolved cells are coping with a basal oxidative stress that control strain cells do not have, and the situation is exacerbated when they are challenged with more oxidative stress in the growth medium. These results appear to disagree with an expected adaptation to oxidative stress after the evolution experiment, although white light resulted a severe growth-impairing stress for parental strain and despite its known effect on generating ROS, the evolved strain did not seem more resistant to oxidative stress but more sensitive. It is noteworthy to point out this slower growth occurred consistently throughout other performed growth assays, *i.e.* different media such as SD, SC and YPG, and different temperatures such as 28, 20 and 12 °C (data not shown), nonetheless further growth tests under different stresses could help establishing a possible adaptive advantage of EVO strain regarding growth performance, in addition to the fitness it has demonstrated under light exposure.

A potential use of the EVO strain for wine fermentation was assessed by testing its fermenting ability on synthetic must (SM). While SM does not fully replicate the chemical complexity and microbiological interactions present in natural grape must, it provides a highly controlled and reproducible environment to evaluate the intrinsic fermentative capacity of a strain (Viana et al., 2014), and the use of airlock valves allowed the semi-anaerobic conditions typically encountered during wine fermentation by allowing CO_2 release while preventing oxygen ingress. Although EVO strain completed the fermentation more slowly than the CONTROL strain (Fig. S2), it was still able to fully consume the available sugars and reach the end of fermentation. This showed its fermentative ability remained competent, opening a potential future application for wine production.

Besides the effects described as a result of light-induced ALE, curious visual traits were observed in EVO strain cultures when grown in SMM under light stress conditions. Such differences encompass a visible brown pigmentation of the cells when grown under light stress and an incipient cell aggregation in liquid culture (Fig. S3). These two phenotypical traits were only exhibited after growth under light-induced stress and the pigmentation seemed to be retained by the cells. SMM without cells was irradiated in parallel and no change of color was observed, remaining transparent.

3.3. Metabolomic analysis

Given the clear phenotypical traits regarding growth performance, cell aggregation, pigmentation and redox state that EVO strain presented in comparison to the CONTROL strain, a metabolomic analysis of both strains was conducted, and both intracellular and extracellular fractions were analyzed. Both strains were grown in darkness, and

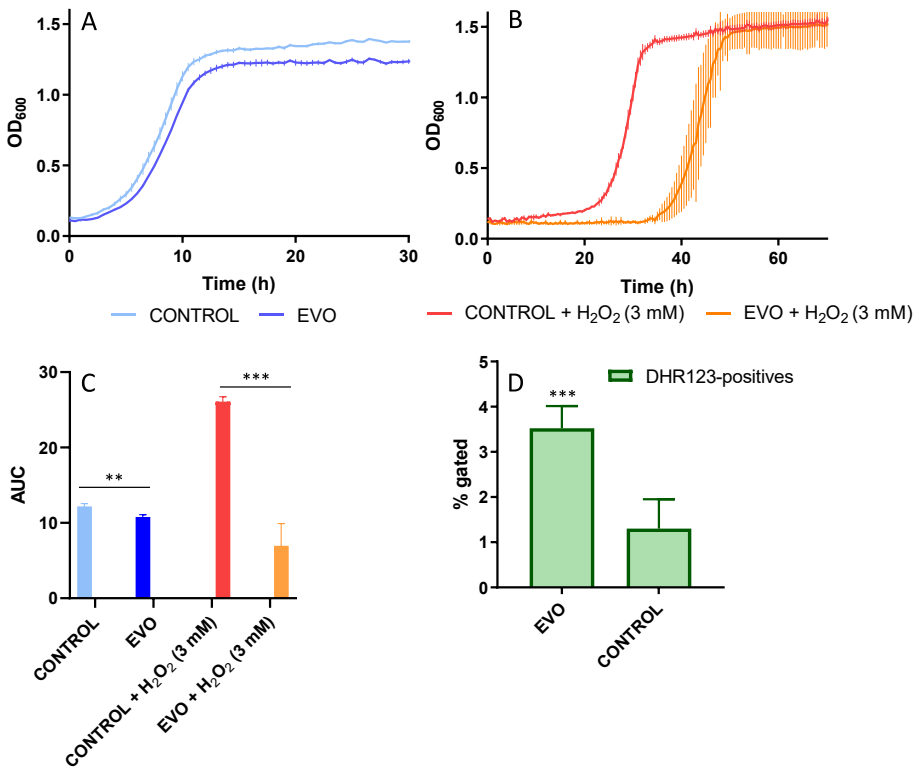

Fig. 2. Growth curves of CONTROL and EVO strains were obtained from growth in SMM at 28 °C (A) and under the same conditions but challenged with H2O2 (B). AUC was calculated at a time where all curves reached stationary phase, being 18 h for unstressed cultures, and 48 h for cultures challenged with H2O2 (C). Intracellular ROS in CONTROL and EVO under no stress condition represented as % of positive-stained cells (D). All results show median values from biological triplicates where error bars represent standard deviation. Asterisks denote significance level from Student's t-test pairwise comparisons ($p < 0.001$ (***), $p < 0.01$ (**)).

additionally EVO strain was grown under white light. This experimental setup yielded three different sample groups, CONTROL, EVO and EVO grown under white light stress (henceforth "LIGHT") and both supernatant and intracellular extract were further analyzed. An untargeted metabolome analysis was performed using a reversed-phase UPLC-ESI (+/−)-QqTOF-MS/MS while a targeted UPLC-MSMS analysis of indolic compounds was additionally conducted for a better metabolomic coverage. Initial data preprocessing from the analysis of the extracellular matrix enabled the identification of a total of 3958 features. Pairwise comparisons between extracted compounds and fragments were made between the three sample sets, and the comparison between CONTROL and EVO showed more differential metabolites than any other, yielding 1009 differential features from which 934 are unique from this comparison (Fig. 3). These results indicate EVO strain was deeply modified through the ALE process and resulted in an altered metabolic state by default in the evolved strain that manifests in a distinct metabolome. Although the differences in growth between the EVO and CONTROL strains across various media are not very pronounced, each strain displays a clearly distinct exometabolome after growing unchallenged due to these differences. The number of differential metabolites is statistically lower when comparing supernatants from EVO and LIGHT samples, revealing an apparent similar metabolomic composition with only 36 exclusive differential metabolites (Fig. 3). Conversely, the comparison between CONTROL and EVO yielded more differential metabolites than comparison between CONTROL and LIGHT, when at least a similar difference was expected between them. This apparent contradiction might be caused by the metabolic state of LIGHT samples, as such stress is provoking active chemical breakdown of metabolites by light photons but also potentially affecting enzymatic activities, transporters and gene expression. These combined effects may add excessive variation in metabolites concentrations across

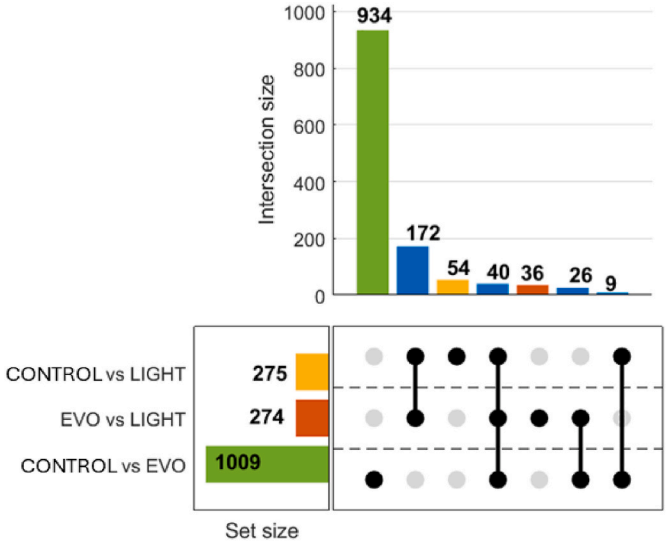

Fig. 3. Upset plot from extracellular UPLC-MS features from the untargeted metabolomic analysis showing the numbers of differential metabolites derived from each comparison and the different intersections between them. 3958 features were analyzed and significant differences in the comparisons in each test have been determined by a *t*-test for unequal variances with a p-value cutoff of 0.05.

replicates, rendering a low significance for most of them in the pairwise comparison, so they can't be accounted in the analysis. This fact challenges the inference on the similarity between EVO and LIGHT using only this data, so a more comprehensive analysis, using transcriptomic

and genomic data is recommended for that purpose.

The analysis of the endometabolome revealed distinct profiles among the sample groups as shown by a Partial Least Squares Discriminant Analysis (PLSDA) model, in which the group of indoles and derivatives, and carboxylic acids and derivatives were of special relevance for the discrimination, among others (Fig. S4).

To better understand the biological relevance of the vast number of differential metabolites and their abundance in the different sample groups, a *mummichog* functional analysis was performed to predict those metabolic pathways that are primarily involved in such differences. In such test differential features were clustered into functional categories as described in Li et al. (2013). Among the differential metabolites in the comparison between CONTROL and EVO metabolomes, a clear representation of "tryptophan metabolism" was observed in both extracellular and intracellular fractions, but also in the exometabolomic comparison between EVO and LIGHT (Fig. 4). Tryptophan metabolism was not the only overrepresented cluster shaping the new aromatic amino acid compound profile in the evolved strain, phenylalanine-related compounds were also enriched in the EVO strain compared to the CONTROL, especially at intracellular level (Fig. 4). Glutathione, arginine, and proline-related metabolites were also differentially detected in EVO strain compared to the CONTROL, which indicates evolved cells are by default producing a higher proportion of molecules with a bioactive potential that play an important role in the non-enzymatic stress response in yeast (Auesukaree, 2017). Metabolites related to tryptophan and glutathione were mainly enriched in the extracellular matrix, while those related to the metabolism of phenylalanine, arginine and proline gained more presence intracellularly. Nonetheless, when challenged with white light, EVO strain showed an enrichment of all these categories even in the extracellular matrix.

After observing a differential overrepresentation of tryptophan-related metabolites and other functional clusters that can be related to the synthesis of antioxidant bioactive molecules in the evolved strain, the focus was set on what specific metabolites of those involved in aromatic amino acid pathways varied between sample groups.

The EVO strain grown in darkness showed a higher concentration of aromatic amino acids (AAA) when compared to the control strain, such as tyrosine, phenylalanine and Trp, and some related metabolites such as kynurenic acid, anthranilate, tyramine and 5-hydroxytryptophol also presented a comparatively higher abundance (Fig. 5 and Table S2). These amino acids are precursors of antioxidant molecules with the potential of modulating gene expression or even scavenge free-radicals, therefore a higher basal concentration of AAAs can presumably predispose evolved cells to cope with an upcoming photo-oxidative stress at different levels.

Despite EVO showed a clearly altered metabolomic profile, the most conspicuous differences involving aromatic amino acids metabolism were triggered by light-induced stress, involving a larger number of related metabolites and larger differences in signal intensity when studying the comparison between sample group LIGHT and EVO (Fig. 5 and Table S3). All the above-mentioned metabolites and additional derivatives and intermediates possess bioactive properties and their relative abundance were different orders of magnitude increased in the evolved strain, especially as a response to light, such as 5-hydroxytryptophan, indole acetaldehyde, 5-hydroxyindoleacetic acid, coumaroylserotonin or indole-5,6-quinone (Fig. 5 and Tables S2 and S3).

It is interesting to note that despite the presence 5-hydroxytryptophan has been previously reported in *S. cerevisiae*, its synthesis is unlikely related to the hydroxylation of L-Trp, being the carboxylation of serotonin a feasible spontaneous reaction instead (Muñiz-Calvo et al., 2019). Similarly, no described mechanisms explain the presence of 5-hydroxyindoleacetic acid or coumaroylserotonin, although both are

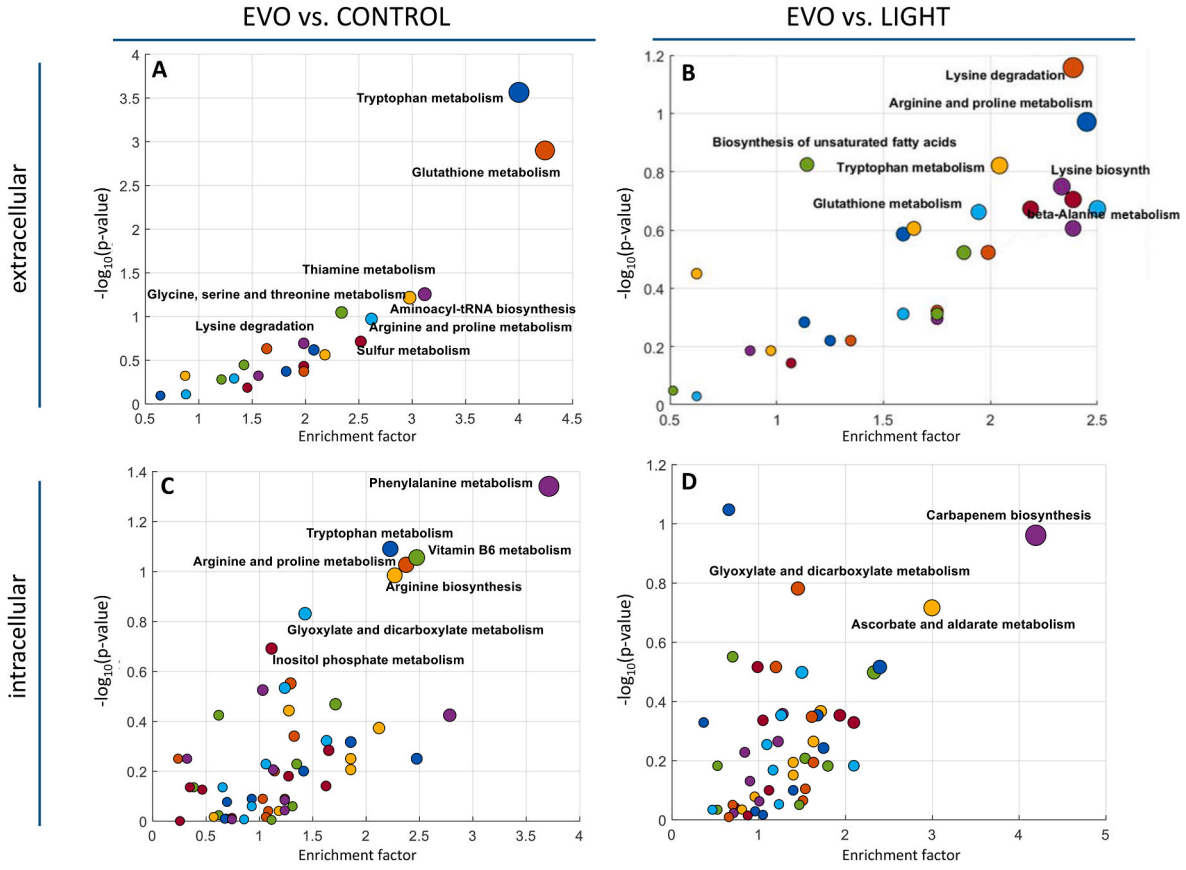

Fig. 4. *Mummichog* analysis from metabolomic analyses representing functional categories identified from comparisons between sample groups using UPLC-MS features classified as "informative" from both extracellular (A and B) and intracellular (C and D) fractions.

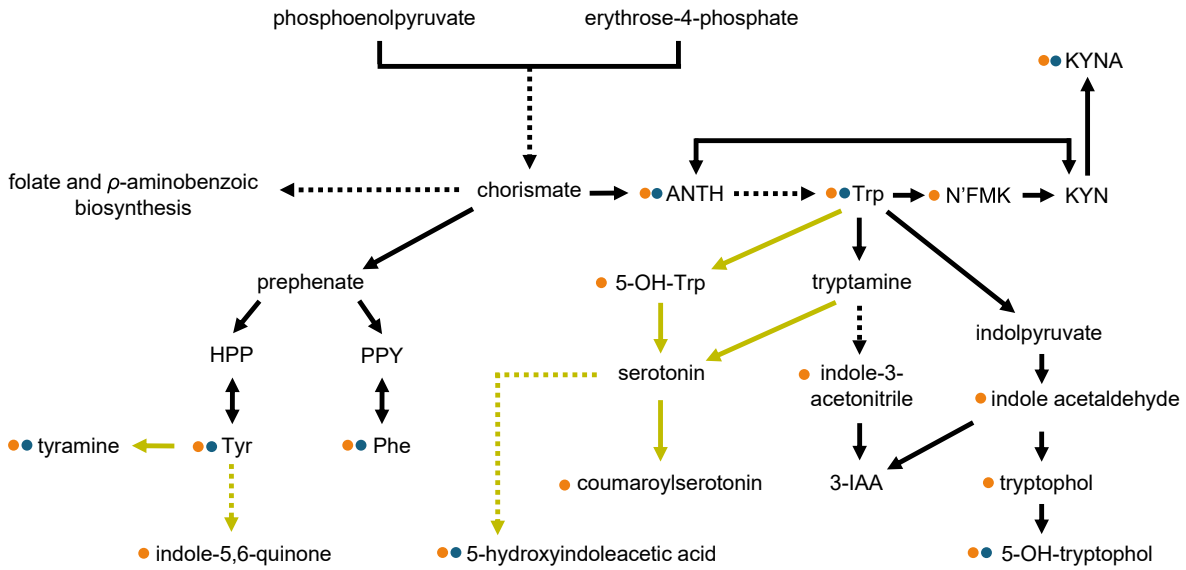

Fig. 5. Aromatic amino acids metabolic pathways. Metabolites that were increased either intracellularly or in the growth media in EVO in comparison to CONTROL are marked with blue, while those increased in LIGHT compared to EVO are marked with orange. Black arrows represent reactions previously reported in yeast while green arrows indicated reactions still not established in yeast. Multiple step reactions are shown as dotted lines. (For interpretation of the references to colour in this figure legend, the reader is referred to the Web version of this article.)

metabolically related to serotonin. Compounds from the untargeted analysis, although identified using isotopic profile and MS/MS spectral matching in a high-accuracy method (Ten-Doménech et al., 2020), need to be carefully considered as putative, as no validation using a pure analytical standard has been carried out for them. The mere inferred occurrence of tyramine and indole-5,6-quinone as result of yeast metabolism is, to date, unprecedented. Indole-5,6-quinone is a known precursor of melanin and, in mammals, it is synthesized from tyrosine by hydroxylation to dihydroxyphenylalanine (DOPA) and subsequent oxidation to dopaquinone. Then it is cyclized to dopachrome and oxidized to indol-5,6-quinone, one of the monomers involved in the eumelanin structure. As it has been recently described, this compound by itself possesses hallmark properties of eumelanin such as a broadband wavelength absorption between 200 and 1000 nm and antioxidant properties, among others (Wang et al., 2023). The ability to produce indole-5,6-quinone as a response to a light stress is a potential adaptive advantage that could explain the capacity of EVO strain to grow under such radiation intensities where CONTROL strain is not able to grow and opens a possible interpretation to the observed pigmentation of cells, as indole-5,6-quinone can be further oxidized and polymerized to form bigger and more stable structures and crystals with optical properties similar to melanin.

Other bioactive indolic compounds derived from the metabolism of serotonin, such as 5-hydroxyindoleacetic acid or coumaroylserotonin are reported to possess a potent antioxidant capacity (Lazari et al., 2017; Mercolini et al., 2012) and the ability to synthesize them can confer yeast cells an adaptive advantage against oxidative stress. The increase of all these metabolites in response to white light suggests a possible metabolic rerouting involving amine decarboxylases and monooxygenases that still remain unknown in yeast. Nevertheless, under white light conditions and, therefore, high ROS levels, spontaneous oxidation of some metabolites may also occur in a non-enzymatic manner favoring the formation of compounds such as 5-hydroxyindoleacetic acid, indole acetaldehyde and indole-5,6-quinone, and thus constituting a passive stress response rather than an active metabolic rerouting.

These results showed that the EVO strain has a distinct profile of bioactive aromatic amino acid-derived compounds as a result of the evolutionary process under white light stress. These metabolomic differences are exacerbated when the cells are challenged with white light, and an increase in these compounds, and specifically indoles, is detected. This supports a relation between the synthesis of indoles and protection against white light-induced stress as it was similarly reported previously for the indolic compound melatonin and its protective effect against UV in yeast (Bisquert et al., 2018).

Outside of the aromatic amino acids metabolism, glutathione relative concentration was halved in the evolved strain compared to CONTROL when both were grown in darkness, suggesting a trade-off between AADC and glutathione synthesis. The lower basal abundance of this ROS-detoxifying molecule in the evolved strain when grown in darkness also agrees with the observed higher intracellular ROS levels determined by flow cytometry (Fig. 2D). For the LIGHT sample group, this tendency is completely reverted. The evolved strain increased the concentration of glutathione, but also of AADCs as seen above, which suggests a light-triggered regulatory switch resulting in a coordinated non-enzymatic stress response.

3.4. *Genetic traits of evolved strain*

In order to determine the extent of the genetic changes produced during white light exposure in the ALE of the EVO strain compared to the CONTROL strain, and to propose possible hypothesis regarding the underlying causes of the new metabolic profile, the genomes of the CONTROL and EVO strains were sequenced, and the sequence polymorphisms resulting from the white light stress ALE process were extracted. Copy number variation (CNV) was established for both strains using S288c genome as a reference, and duplications and deletions were established for both CONTROL and EVO strains. The largest structural differences between both strains are an extensively duplicated region of approximately 60 % of chromosome VII in EVO strain that is not present in CONTROL and large duplications in chromosomes I, III and VI of CONTROL that occur exclusively in this strain (Fig. S5). Chromosomal gain and loss, as well as large rearrangements are common mechanisms of adaptation to stresses and new environments in yeast, but the biological consequences of these big structural changes must be evaluated together with the study of the phenotypes and gene expression analysis (Chang et al., 2013; Mangado et al., 2018). The evolution experiment resulted in significant structural changes, as mentioned above, and that also extends to point mutations across the whole genome. A total of 2471 single nucleotide polymorphisms (SNP) were identified in EVO strain

compared to CONTROL strain, affecting over 800 open reading frames (ORFs). The occurrence of these SNP's is spread across all chromosomes, 1277 in heterozygosity and 1194 in homozygosity, and they displayed regions with a high density of SNPs in chromosomes IV, VII, X and XV (Fig. 6). The high number of SNPs accumulated in EVO in comparison to CONTROL strain was favored by the experimental design as the yeast populations underwent through all of the growth phases to maximize genetic diversity, reaching stationary phase, which itself constitutes a source of cellular stress due to nutrient depletion and a higher ROS generation. These stressors, which are unrelated to the chosen selective pressure, may promote fixing SNPs that are not necessarily beneficial mutations. Nonetheless, the great SNP count difference between both CONTROL and EVO suggests that white light is not only a severe stress for its photo-oxidative effect, but it could also have a strong mutagenic effect in the yeast genome.

Due to the broad distribution of SNPs across multiple ORFs, initial efforts were directed toward identifying potential associations between the observed genetic changes and prominent phenotypic traits with the objective of proposing new hypotheses that help elucidate the underlying genetical structure of these new features. These included the higher production of aromatic amino acid-derived metabolites, the increased cell adhesion and pigmentation following white light exposure, and the ability to grow under light-induced stress conditions. The 885 ORFs carrying one or more non-synonymous mutations were examined and among them, genes involved in the aromatic amino acids pathways were affected. Single nucleotide changes in promoter regions for genes related to these pathways were also found. Among the AADC-related genes with non-synonymous mutations inside the coding region, we highlight *ADH1* (alcohol dehydrogenase), which has a substitution of valine for isoleucine at position 59 in one allele and a substitution of valine for alanine at position 59 in the other allele, and *NMA2* (Nicotinic acid mononucleotide adenylyltransferase), which has a substitution of valine for glycine at position 112 in both alleles (Table 1). An eventual alteration of the function of *NMA2* can directly impact on NAD^+ biosynthesis and regeneration which directly supports the tryptophan catabolism via the kynurenine pathway. Furthermore, *ADH1* directly impacts acetaldehydes consumption that can lead to acids (oxidation) or alcohols (reduction), potentially influencing the pool of AADCs such as indole acetaldehyde or tryptophol and 5-

Table 1
Summary of nonsynonymous mutations identified in genes related to the observed phenotype in the evolved strain.

Gene	Mutations identified in evolved strain
ADH1	V59I/V59A
NMA2	V112G
TRP2	K225E
ARO1	E219A |L1148P
SFL1	N512D | A658V |V679A |R766M
FLO8	M86T |K585E
FLO10	K70Q |G197V
FLO11	Y152H |N188D |H417L |L419H |P454L |Q480P |P499L |H504L |L506H | L519F
INN1	N308D |C388S
CLA4	K285M |P303R
EGT2	H283D

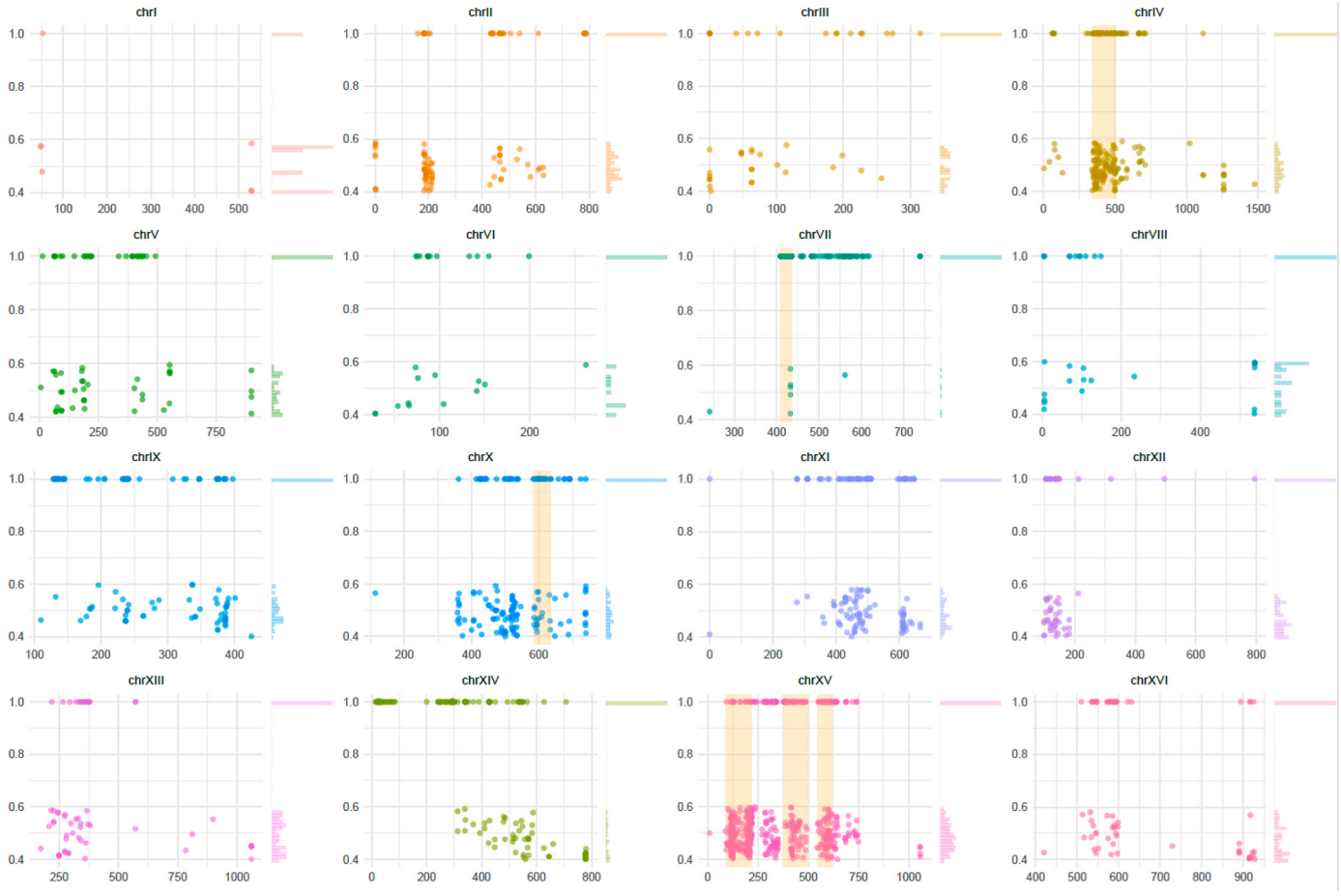

Fig. 6. SNP distribution across the different chromosomes represented as coloured dots using the genomic coordinates in the x axes and the observed frequency in the y axes for EVO strain compared to CONTROL. High-SNP density regions are highlighted. Variations in heterozygosis displayed a frequency close to 0.5 due to the diploid nature of the strains.

hydroxytryptophol. An amino acid substitution (K225E) was also found in *TRP2* gene, encoding anthranilate synthase. Mutated alleles of *TRP2* causing feedback-resistant enzyme forms have been reportedly shown to increase the flux to tryptophan (Graf et al., 1993), nevertheless the specific mutation observed in this study has not been previously assessed. The study of how this point mutation could affect deregulation or affinity modification of this enzyme would clarify *TRP2* role in the increased levels of tryptophan, or downstream metabolites observed in the evolved strain. Mutations in genes upstream the shikimate pathway were also found in shikimate dehydrogenase *ARO1*, which accumulated two-point mutations in the coding region (E219A and L1148P). Regardless of the mutations found in the ORFs of AADC pathways, random mutations on other regulatory systems must be taken into account as partially responsible of the observed phenotypes. Nevertheless, all mutations proposed as potentially linked to these phenotypes remain to be empirically validated in isolation, a task that extends beyond the scope of the present study. This validation will allow to segregate SNPs that are directly contributing to the higher synthesis of AADCs from those occurring randomly across the genome.

Other mutations affecting genes that can be decisive for the observed phenotype of the aggregated cell growth were observed, especially those affecting flocculation-related genes *SFL1*, *FLO8, FLO10* and *FLO11*, which accumulate different nonsynonymous mutations on their coding region (Table 1). During biofilm formation, yeast cells exhibit a similar aggregated pattern as a first step, then they adhere to other cells and surfaces (Bojsen et al., 2012).

The transcriptional levels of *FLO11* and the number of its repeated sequences have been previously linked to differences in in the biofilm-forming ability of *S. cerevisiae* strains (Zara et al., 2009). This gene encodes a glycosylphosphatidylinositol-anchored cell surface flocculin protein, and it is reportedly involved in filamentous growth, invasive growth, biofilm formation and cell adhesion (Avbelj et al., 2016).

Another plausible determinant of the observed aggregation of the yeast cells when grown in liquid media could be a defect in the bud morphogenesis, septum formation and cytokinesis that is preventing the daughter cells to effectively separate from the mother cells and originating these cell aggregates. Genes *INN1*, *CLA4* and *EGT2* play an important role in these functions, and a partial or total loss of function could result in the observed phenotype. This cell-aggregation pattern could provide a competitive advantage against white light radiation by creating a shielded microenvironment in which the exterior cells of the clumps would sustain most of the damage, particularly if they produce a pigment. The induction of cell aggregation has been previously reported in other unicellular organisms such as *Sulfolobus sp*., in which the cell aggregation not only provides a protected micro-environment, but also favors the activity of DNA repair mechanisms and DNA exchange (Götz et al., 2007; Wagner et al., 2017; Wani et al., 2022).

In *S. cerevisiae*, the aromatic higher-alcohols (tryptophol, tyrosol and 2-phenyl ethanol) have been identified as quorum-sensing molecules. These molecules induced a collective growth behavior with advantages for the population as a group such as biofilm formation (Bassler, 1999). Moreover, González et al. (2018) also reported an influence of tryptophan-derived molecules, such as serotonin and tryptamine, in triggering filamentous growth. Therefore, our metabolomic and genomic data support the idea of a possible adaptation to white light stress through punctual mutations in genes that overproduce aromatic amino acid-derived compounds, as well as in the target genes induced by these molecules. This change in growth pattern to filamentous growth must protect the cells from strong light damage.

3.5. Global analysis of gene expression

The global gene expression of CONTROL, EVO and LIGHT samples was analyzed, as described above, to further explore the differences between strains (EVO vs. CONTROL) at the transcript level, but also to study what genes are differentially expressed in response to white light (LIGHT vs. EVO). A summary with the differentially expressed genes (DGE) was obtained as a list for each comparison, and for each comparison, a gene clustering analysis was performed based on gene ontology (GO) terms and the Kyoto Encyclopedia of Genes and Genomes (KEGG) pathway database. At a transcriptomic level the three sample groups were clearly differentiated in a principal component analysis (PCA), showing the differences in the transcriptomic response not only accounted for strain differences, but also for conditions, in this case darkness or light (Fig. S6). The applied significance cutoff resulted in 1763 and 1517 DEGs for EVO vs. CONTROL and LIGHT vs. EVO comparisons, respectively (Tables S4 and S5). The DEGs from the EVO vs CONTROL comparison were particularly enriched in GO terms such as flocculation and cell adhesion (Fig. 7A, Table S6), among them, genes *FLO1*, *FLO9*, *FLO11*, *FLO5*, *SNF1* and *CCW12* were significantly overexpressed in the evolved strain with log-fold change (logFC) values ranging from 0.7 (*CCW12*) to 8.5 (*FLO11*) (Table S4). This result suggests that the mutations observed in these genes impact their transcriptional activity, which reinforces the evolved strain's cell aggregation or filamentous growth strategy. Interestingly, an enrichment of 118 DEGs involved in secondary metabolites biosynthesis (KEGG ID sce01110) was observed in this comparison, among them, genes with a potential impact on aromatic amino acid metabolism such as *ARO7* (logFC 1.18), *ADH1* (logFC 0.91), *ADH3* (logFC 0.61) and *ADH6* (logFC 0.97) were overexpressed in EVO (Fig. 7B–Tables S4 and S6). Apart from these gene clusters that can contribute directly to cell aggregation phenotypes or increased concentrations of AADC, the activation of genes upstream of the AAA pathways, such as those belonging to the pentose phosphate pathway (PPP) or general sucrose and maltose metabolism, were also upregulated in EVO compared to CONTROL. Such activation in upstream carbon source mobilization genes can be determinant for providing enough substrate for the AADCs produced downstream. In relation to the observed phenotype, more specifically on the higher ROS levels detected in the evolved strain when compared to the control, a strong repression of *CTA1* (logFC −4.7) was detected in EVO, which can explain its basal ROS levels and poor growth performance when challenged with H_2O_2, as mitochondrial catalase constitutes a major line of defense against this stress. This underscores ALE against white light in this case did not favor a complete oxidative stress-directed adaptation, but a photo-specific tolerance acting on mechanisms related to oxidative stress response such as increasing AAA pool and glutathione in response to light, but not exclusively, as other phenotypes with a physical shielding potential such as cell aggregation and pigmentation concurrently arose.

In regard to the LIGHT vs. EVO comparison, an enrichment of genes related to sulfur metabolism was observed, together with transmembrane transport and sugars catabolism, most of the DEGs in these categories were also clustered under “biosynthesis of secondary metabolites” according to KEGG pathway database, grouping up to 117 genes (Fig. 7CD, Table S7). Genes overexpressed in response to white light in the evolved strain, such as *MET3* (logFC 2.68), *MET14* (logFC 2.98), *MET16* (logFC 2.96), *MET5* (logFC 2.49) and *MET10* (logFC 2.40), together with *CYS4* (logFC 1.38), *CYS3* (logFC 1.90), *SSU1* (logFC 0.96), *SAM2* (logFC 2.03) and *SAM3* (logFC 0.98), suggest that under this condition, the cell strongly activates the sulfate assimilation machinery and the sulfite detoxification, boosting the synthesis of *S*-adenosylmethionine and cysteine, and ultimately adjusting the redox balance and increasing glutathione biosynthesis, as it was observed in the analysis of the exometabolome for LIGHT sample group. Moreover, as determined in the metabolomic analysis, AADCs proportionally increased in response to white light in the evolved strain, and a transcriptomic effect on genes related to the metabolism of AAA family was also found, highlighting the overexpression of *ARO10*, *PDC5*, *PDC6*, *ARO9* and *BNA2* with high logFC values up to 4.48 for *ARO10*, or 3.19 in the case of *ARO9*, among others (Table S5).

The mechanism underlying DEGs in the EVO strain in comparison to CONTROL, or those conditioned by white light is likely to be the result of

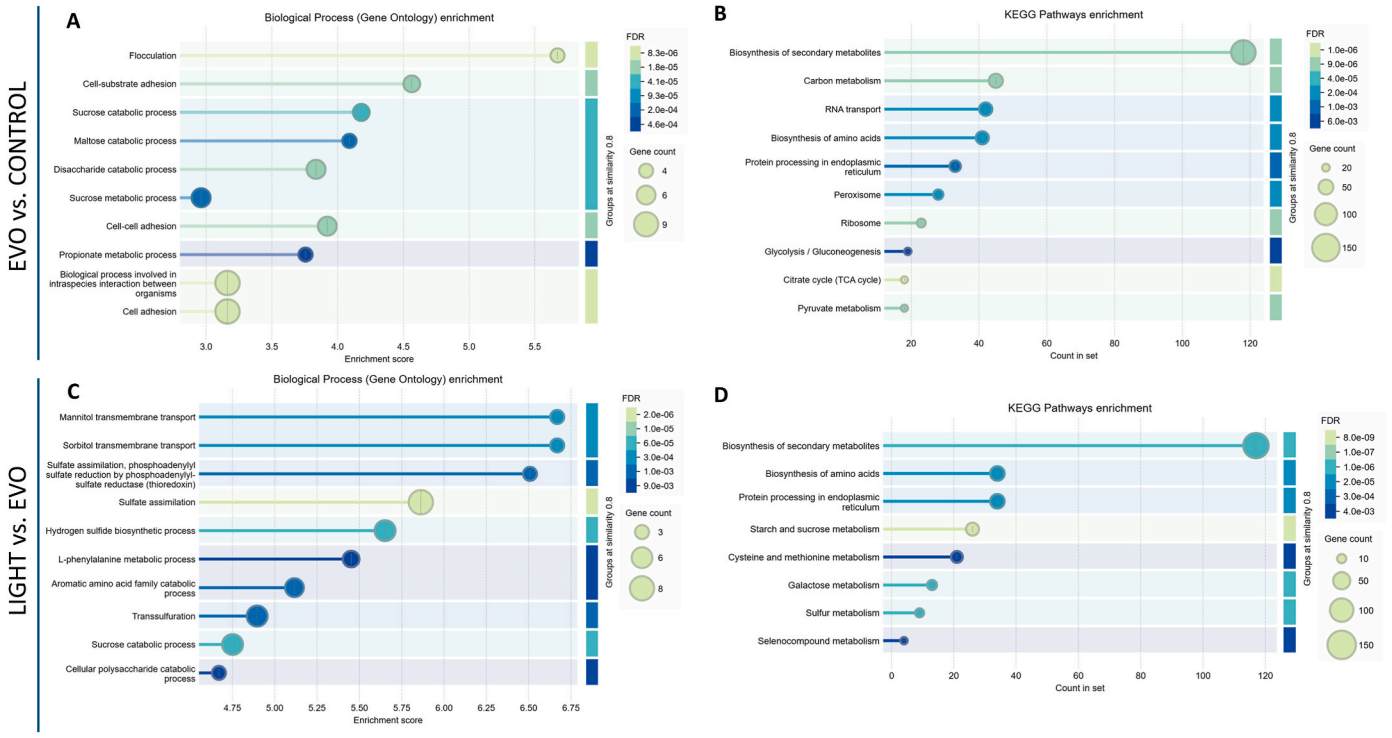

Fig. 7. Functional enrichment analyses performed on DEGs derived from the RNAseq analysis for the comparisons EVO vs. CONTROL and LIGHT vs. EVO highlighting gene ontology (GO) terms (A, and C) and KEGG Pathways categories (B and D).

multiple factors such as stress response, regulation networks and structural changes affecting the different ORFs. In relation to the structural changes affecting the ORFs, in the gene *ADH1*, overexpressed in EVO in relation to CONTROL under the same conditions, an amino acid substitution of V59 for an alanine or an isoleucine was found, and it should be considered to study a possible deregulation of its activity. Furthermore, one of the notoriously overexpressed gene family in response to white light, *MET5*, accumulated two amino acid substitutions I604V and T712I, with a potential interest in the study of the sulfate assimilation process and the resistance to sulfite. Among further upregulated genes discussed above and related to large structural changes, *PDC6* and *CYS4* are both in the duplicated region of chromosome VII, but their overexpression was only determined as a response to light.

4. Conclusions

The obtention of new yeast strains with the capacity of increasing bioactive compounds in wine or other fermented beverages is of great interest. Recently the presence of AADCs such as serotonin and melatonin or their derivatives in wines and their attribution to yeast metabolism has prompted the search of effective methods to improve yeast ability to increase the amount of these interesting compounds. The biosynthesis of some of the most interesting compounds such as hydroxytyrosol, melatonin or serotonin still remain unknown in yeast, and the use of a non-GMO approach contributes to the arduousness of selecting a stimulus to push yeast metabolism towards their synthesis. In this work, an adaptive laboratory evolution experiment was performed on a wine yeast using a novel selective pressure based on white light irradiation to generate a stress by photooxidation. It has been reported that visible light alters yeast metabolic rhythms by inhibiting respiration and by producing reactive oxygen species that up-regulate the oxidative stress response (Robertson et al., 2013). After 170 generations, yeast strain subjected to directed evolution was able to proficiently grow under a PAR radiation dose 10 times higher than the dose which inhibits growth of the parental strain, revealing a clear adaptation to this stress. Contrary to what was expected, adaption to photooxidation doesn't seem to improve the strain's fitness against oxidative stress when challenged with hydrogen peroxide. While still maintaining an acceptable growth and a synthetic grape-must fermentation capacity, a slight delay compared to the control strain was observed together with a higher intracellular ROS level. The higher basal ROS in EVO strain is likely multifactorial, consistent with a high metabolic burden from a constitutively active non-enzymatic response (increased AADC production and higher AAA precursor pool), but also from the severe gene repression on its mitochondrial catalase *CTA1*. These features underline a trade-off where they slightly impact general fitness under normal conditions but allow outstanding survival and growth under white light stress.

An initial metabolomic analysis on control and evolved strain grown in darkness and under white light conditions, revealed great differences between CONTROL and EVO. Some of the most significant differences involved an increase in tryptophan-related metabolites such as indolic compounds, finding interesting bioactive or bioactive precursors increased due to EVO metabolism such as 5-hydroxytryptophol, anthranilate, 5-hydroxyindoleacetic acid, and kynurenic acid (Table S2). Growth under white light stress was associated with a distinctive phenotype characterized by mild cell aggregation and pigmentation. Additionally, this condition triggered the synthesis of more antioxidant metabolites in EVO strain such as glutathione, serotonin derivates and aromatic amino acids phenylalanine, tyrosine and tryptophan (Table S3). Among the white light-triggered overproduced metabolites, indole-5,6-quinone is of special relevance, due to its antioxidant and photoprotective properties, which are known to be shared with those of the pigment eumelanin. The synthesis of indole-5,6-quinone, but also coumaroylserotonin, both identified in EVO strain after growth under white light, require a monooxygenase to catalyze the conversion of tyrosine to L-DOPA, and the production of p-coumaric acid from cinnamate, respectively. Their finding of this trait in the EVO strain is important because it could provide new insights into the genetic determinants of cytochrome P450 monooxygenases in the budding

yeast. This is a very limited superfamily of monooxygenases, with only a few representatives in *S. cerevisiae*. Therefore, a complete directed and quantitative analysis using pure analytical standards should be conducted to validate and quantify these interesting metabolites. Another evident trait of the EVO strain is the change in its growth mode, displaying aggregate growth that can protect the shielded cells against photooxidative damage due to white light.

The sequencing of both parental and evolved strain allowed us to detect genetic variations on genes involved in the metabolic pathways of the increased metabolites and propose possible hypothesis on the mechanisms behind the observed phenotypes. The described mutations entailed amino acids substitutions in a small number of genes that may affect the observed phenotype and therefore they will be isolatedly tested on the control strain to assess their potential individual impact on the phenotype in following studies. The observed genomic changes correlated nonetheless with an increased transcription activity of the genes involved in the synthesis of aromatic amino acid-derived compounds as well as other genes involved in flocculation, cell aggregation and in oxidative stress response. With regard to this latter metabolic trait, the large number of genes involved in sulfur amino acid metabolism that were up-regulated in cells challenged by white light was noteworthy. Previous work by García-Ríos et al. (2014) observed similar upregulation of genes in the sulfur assimilation pathway and glutathione biosynthesis in yeast cells growing at low temperatures. It has been demonstrated that this pathway's upregulation is an adaptive strategy to counteract higher oxidative stress at low temperatures and increase *S*-adenosylmethionine (SAM) production, a key metabolite in phospholipid synthesis. Similarly, we hypothesize that light damage to cells also induces an oxidative stress response and reshapes the plasma membrane configuration, increasing the demand for phospholipids.

To the best of our knowledge, this is the first report on the phenotypic, metabolomic and genomic changes undergone by a *S. cerevisiae* strain after many generations of growth in the presence of white light as a stressor. Although exposure of cells to visible light from natural or artificial sources is generally considered relatively innocuous, the deep genomic changes observed following the ALE process reveal the mutagenic potential of white light and its future potential for generating significant genetic variability among *S. cerevisiae* strains. We also consider the ultimate goal of this ALE strategy, enhancing the synthesis of bioactive aromatic amino acid-derived compounds in the evolved strain, to be very novel, as it has been proven to be a correct hypothesis. Therefore, we believe that this work could pave the way for the future development of new strains with enhanced synthesis of these interesting metabolites, which could be used in fermented foods and beverages. At the same time, our results open up new avenues for unveiling the pathways involved in some of these metabolites that have not yet been linked to yeast metabolism, as well as the genes that encode the enzymes of these undisclosed pathways.

CRediT authorship contribution statement

Ricardo Bisquert: Writing – original draft, Visualization, Methodology, Investigation. **Alba Guillén:** Investigation. **Guillermo Quintas:** Methodology, Formal analysis, Data curation. **José M. Guillamón:** Writing – review & editing, Supervision, Funding acquisition.

Funding

This work was funded by MCIN/AEI/10.13039/501100011033, grant number PID2022-142748OB-I00. RB and AG thank their respective BES-2017-079640 and PRE2020-093597 grants funded by MCIN/AEI. Authors acknowledge the award of the Spanish government MCIN/AEI to the IATA-CSIC as Center of Excellence (CEX2021-001189-S/MICIU/AEI/10.13039/501100011033).

Declaration of competing interest

The authors declare that they have no known competing financial interests or personal relationships that could have appeared to influence the work reported in this paper.

Appendix A. Supplementary data

Supplementary data to this article can be found online at https://doi.org/10.1016/j.fm.2026.105295.

Data availability

The primary datasets used in the preparation of this manuscript and their analyses are openly available in Digital CSIC (http://hdl.handle.net/10261/403811)

References

Aarnio, T.H., Suihko, M.L., Kauppinen, V.S., 1991. Isolation of acetic acid-tolerant Baker's yeast variants in a turbidostat. Appl. Biochem. Biotechnol. 27 (1), 55–63. https://doi.org/10.1007/BF02921515.

Andrews, S., 2010. FastQC: a quality control tool for high throughput sequence data. https://www.bioinformatics.babraham.ac.uk/projects/fastqc/. Available online at:

Auesukaree, C., 2017. Molecular mechanisms of the yeast adaptive response and tolerance to stresses encountered during ethanol fermentation. J. Biosci. Bioeng. 124 (2), 133–142. https://doi.org/10.1016/j.jbiosc.2017.03.009.

Avbelj, M., Zupan, J., Raspor, P., 2016. Quorum-sensing in yeast and its potential in wine making. Appl. Microbiol. Biotechnol. 100 (18), 7841–7852. https://doi.org/10.1007/s00253-016-7758-3.

Ballester-Tomás, Lidia, Randez-Gil, Francisca, Pérez-Torrado, Roberto, Prieto, Jose Antonio, 2015. Redox engineering by ectopic expression of glutamate dehydrogenase genes links NADPH availability and NADH oxidation with cold growth in Saccharomyces cerevisiae. Microbial Cell Factories 14 (1), 100. https://doi.org/10.1186/s12934-015-0289-2. http://microbialcellfactories.biomedcentral.com/articles/10.1186/s12934-015-0289-2. (Accessed 9 July 2015).

Bassler, Bonnie L, 1999. How bacteria talk to each other: regulation of gene expression by quorum sensing. Current Opinion in Microbiology 2 (6), 582–587. https://doi.org/10.1016/s1369-5274(99)00025-9. https://linkinghub.elsevier.com/retrieve/pii/S1369527499000259.

Bisquert, R., Muñiz-Calvo, S., Guillamón, J.M., 2018. Protective role of intracellular melatonin against oxidative stress and UV radiation in Saccharomyces cerevisiae. Front. Microbiol. 9 (FEB), 1–11. https://doi.org/10.3389/fmicb.2018.00318.

Bodvard, K., Peeters, K., Roger, F., Romanov, N., Igbaria, A., Welkenhuysen, N., Palais, G., Reiter, W., Toledano, M.B., Käll, M., Molin, M., 2017. Light-sensing via hydrogen peroxide and a peroxiredoxin. Nat. Commun. 8. https://doi.org/10.1038/ncomms14791.

Bojsen, R.K., Andersen, K.S., Regenberg, B., 2012. Saccharomyces cerevisiae - a model to uncover molecular mechanisms for yeast biofilm biology. FEMS Immunol. Med. Microbiol. 65 (2), 169–182. https://doi.org/10.1111/j.1574-695X.2012.00943.x.

Chang, S.L., Lai, H.Y., Tung, S.Y., Leu, J.Y., 2013. Dynamic large-scale chromosomal rearrangements fuel rapid adaptation in yeast populations. PLoS Genet. 9 (1). https://doi.org/10.1371/journal.pgen.1003232.

Chen, Shifu, Zhou, Yanqing, Chen, Yaru, Gu, Jia, 2018. fastp: an ultra-fast all-in-one FASTQ preprocessor. Bioinformatics 34 (17), i884–i890. https://doi.org/10.1093/bioinformatics/bty560. https://academic.oup.com/bioinformatics/article/34/17/i884/5093234. (Accessed 8 September 2018).

Cordente, A.G., Schmidt, S., Beltran, G., Torija, M.J., Curtin, C.D., 2019. Harnessing yeast metabolism of aromatic amino acids for fermented beverage bioflavouring and bioproduction. Appl. Microbiol. Biotechnol. 103 (11), 4325–4336. https://doi.org/10.1007/s00253-019-09840-w.

Fernández-Cruz, E., Álvarez-Fernández, M.A., Valero, E., Troncoso, A.M., García-Parrilla, M.C., 2016. Validation of an analytical method to determine melatonin and compounds related to l-Tryptophan metabolism using UHPLC/HRMS. Food Anal. Methods 9 (12), 3327–3336. https://doi.org/10.1007/s12161-016-0529-z.

García-Ríos, E., Lairón-Peris, M., Ortiz-Julien, A., Poirot, P., Rozès, N., Querol, A., Guillamón, J.M., 2022. Thermo-adaptive evolution to generate improved Saccharomyces cerevisiae strains for cocoa pulp fermentations. Int. J. Food Microbiol. 342 (January 2021). https://doi.org/10.1016/j.ijfoodmicro.2021.109077.

García-Ríos, E., López-Malo, M., Guillamón, M.M., 2014. Global phenotypic and genomic comparison of two Saccharomyces cerevisiae wine strains reveals a novel role of the sulfur assimilation pathway in adaptation at low temperature fermentations. BMC Genom. 15 (1), 1–18. https://doi.org/10.1186/1471-2164-15-1059.

González, Beatriz, Vázquez, Jennifer, Cullen, Paul J., Mas, Albert, Beltran, Gemma, Torija, María-Jesús, 2018. Aromatic Amino Acid-Derived Compounds Induce Morphological Changes and Modulate the Cell Growth of Wine Yeast Species. Frontiers in Microbiology 9, 670. https://doi.org/10.3389/fmicb.2018.00670. http://journal.frontiersin.org/article/10.3389/fmicb.2018.00670/full. (Accessed 11 April 2018).

Gonzalez, R., Morales, P., 2022. Truth in wine yeast. Microb. Biotechnol. 15 (5), 1339–1356. https://doi.org/10.1111/1751-7915.13848.
Götz, D., Paytubi, S., Munro, S., Lundgren, M., Bernander, R., White, M.F., 2007. Responses of hyperthermophilic crenarchaea to UV irradiation. Genome Biol. 8 (10). https://doi.org/10.1186/gb-2007-8-10-r220.
Graf, R., Mehmann, B., Braus, G.H., 1993. Analysis of feedback-resistant anthranilate synthases from Saccharomyces cerevisiae. J. Bacteriol. 175 (4), 1061–1068. https://doi.org/10.1128/jb.175.4.1061-1068.1993.
Lario, S., Ramírez-Lázaro, M.J., Sanjuan-Herráez, D., Brunet-Vega, A., Pericay, C., Gombau, L., Junquera, F., Quintás, G., Calvet, X., 2017. Plasma sample based analysis of gastric cancer progression using targeted metabolomics. Sci. Rep. 7 (1), 1–10. https://doi.org/10.1038/s41598-017-17921-x.
Lazari, D., Alexiou, G.A., Markopoulos, G.S., Vartholomatos, E., Hodaj, E., Chousidis, I., Leonardos, I., Galani, V., Kyritsis, A.P., 2017. N-(p-coumaroyl) serotonin inhibits glioblastoma cells growth through triggering S-phase arrest and apoptosis. J. Neuro Oncol. 132 (3), 373–381. https://doi.org/10.1007/s11060-017-2382-3.
Li, S., Park, Y., Duraisingham, S., Strobel, F.H., Khan, N., Soltow, Q.A., Jones, D.P., Pulendran, B., 2013. Predicting network activity from high throughput metabolomics. PLoS Comput. Biol. 9 (7). https://doi.org/10.1371/journal.pcbi.1003123.
Mangado, A., Morales, P., Gonzalez, R., Tronchoni, J., 2018. Evolution of a yeast with industrial background under winemaking conditions leads to diploidization and chromosomal copy number variation. Front. Microbiol. 9 (AUG), 1–12. https://doi.org/10.3389/fmicb.2018.01816.
Marhuenda, J., Medina, S., Martínez-Hernández, P., Arina, S., Zafrilla, P., Mulero, J., Genieser, H.G., Ferreres, F., Gil-Izquierdo, Á., 2016. Melatonin and hydroxytyrosol-rich wines influence the generation of DNA oxidation catabolites linked to mutagenesis after the ingestion of three types of wine by healthy volunteers. Food Funct. 7 (12), 4781–4796. https://doi.org/10.1039/c6fo01246a.
Martínez-Sena, T., Luongo, G., Sanjuan-Herráez, D., Castell, J.V., Vento, M., Quintás, G., Kuligowski, J., 2019. Monitoring of system conditioning after blank injections in untargeted UPLC-MS metabolomic analysis. Sci. Rep. 9 (1), 1–9. https://doi.org/10.1038/s41598-019-46371-w.
Matsutani, K., Fukuda, Y., Murata, K., Kimura, A., Yajima, N., 1992. Adaptation mechanism of yeast to extreme environments: construction of salt-tolerance mutants of the yeast Saccharomyces cerevisiae. J. Ferment. Bioeng. 73 (3), 228–229. https://doi.org/10.1016/0922-338X(92)90166-R.
Mercolini, L., Mandrioli, R., Raggi, M.A., 2012. Content of melatonin and other antioxidants in grape-related foodstuffs: measurement using a MEPS-HPLC-F method. J. Pineal Res. 53 (1), 21–28. https://doi.org/10.1111/j.1600-079X.2011.00967.x.
Muñiz-Calvo, S., Bisquert, R., Fernández-Cruz, E., García-Parrilla, M.C., Guillamón, J.M., 2019. Deciphering the melatonin metabolism in Saccharomyces cerevisiae by the bioconversion of related metabolites. J. Pineal Res. 66 (3), 1–9. https://doi.org/10.1111/jpi.12554.
Novo, M., Gonzalez, R., Bertran, E., Martínez, M., Yuste, M., Morales, P., 2014. Improved fermentation kinetics by wine yeast strains evolved under ethanol stress. Lwt 58 (1), 166–172. https://doi.org/10.1016/j.lwt.2014.03.004.
Planells-Cárcel, A., Sánchez-Martí, S., Muñiz-Calvo, S., Guillamon, J.M., 2025. IAT4, a new indolamine N-Acetyltransferase in Saccharomyces cerevisiae involved in melatonin biosynthesis. J. Pineal Res. 77 (3). https://doi.org/10.1111/jpi.70053.
Planells-Cárcel, Andrés, Kazakova, Julia, Pérez, Cristina, Gonzalez-Ramirez, Marina, Garcia-Parrilla, M. Carmen, Guillamón, José M., 2024. A consortium of different Saccharomyces species enhances the content of bioactive tryptophan-derived compounds in wine fermentations. International Journal of Food Microbiology 416, 110681. https://doi.org/10.1016/j.ijfoodmicro.2024.110681. https://linkinghub.elsevier.com/retrieve/pii/S0168160524001259, 110681.
Querol, A., Barrio, E., Ramón, D., 1992. A comparative study of different methods of yeast strain characterization. Syst. Appl. Microbiol. 15 (3), 439–446. https://doi.org/10.1016/S0723-2020(11)80219-5.
Riou, C., Valancogne, C., Pieri, P., 1989. Un modèle simple d'interception du rayonnement solaire par la vigne - vérification expérimentale. Agronomie 9 (5), 441–450. https://doi.org/10.1051/agro:19890502.
Robertson, J.B., Davis, C.R., Johnson, C.H., 2013. Visible light alters yeast metabolic rhythms by inhibiting respiration. Proceedings of the National Academy of Sciences of the United States of America 110 (52), 21130–21135. https://doi.org/10.1073/pnas.1313369110.
Rodriguez-Naranjo, M.I., Gil-Izquierdo, A., Troncoso, A.M., Cantos-Villar, E., Garcia-Parrilla, M.C., 2011. Melatonin is synthesised by yeast during alcoholic fermentation in wines. Food Chem. 126 (4), 1608–1613. https://doi.org/10.1016/j.foodchem.2010.12.038.
Sánchez-Illana, Á., Piñeiro-Ramos, J.D., Sanjuan-Herráez, J.D., Vento, M., Quintás, G., Kuligowski, J., 2018. Evaluation of batch effect elimination using quality control replicates in LC-MS metabolite profiling. Anal. Chim. Acta 1019, 38–48. https://doi.org/10.1016/j.aca.2018.02.053.
Takagi, H., Iwamoto, F., Nakamori, S., 1997. Isolation of freeze-tolerant laboratory strains of Saccharomyces cerevisiae from proline-analogue-resistant mutants. Appl. Microbiol. Biotechnol. 47 (4), 405–411. https://doi.org/10.1007/s002530050948.
Ten-Doménech, I., Martínez-Sena, T., Moreno-Torres, M., Sanjuan-Herráez, J.D., Castell, J.V., Parra-Llorca, A., Vento, M., Quintás, G., Kuligowski, J., 2020. Comparing targeted vs. untargeted MS2 data-dependent acquisition for peak annotation in LC–MS metabolomics. Metabolites 10 (4). https://doi.org/10.3390/metabo10040126.
Tilloy, V., Ortiz-julien, A., 2014. Reduction of Ethanol Yield and Improvement of Glycerol Formation by Adaptive Evolution of the Wine Yeast Saccharomyces cerevisiae under Hyperosmotic Conditions, vol. 80, pp. 2623–2632. https://doi.org/10.1128/AEM.03710-13, 8.
Vázquez, J., González, B., Sempere, V., Mas, A., Torija, M.J., Beltran, G., 2017. Melatonin reduces oxidative stress damage induced by hydrogen peroxide in Saccharomyces cerevisiae. Front. Microbiol. 8 (JUN), 1–14. https://doi.org/10.3389/fmicb.2017.01066.
Viana, Tiago, Loureiro-Dias, Maria C, Prista, Catarina, 2014. Efficient fermentation of an improved synthetic grape must by enological and laboratory strains of Saccharomyces cerevisiae. AMB Express 4 (1), 16. https://doi.org/10.1186/s13568-014-0016-0. https://amb-express.springeropen.com/articles/10.1186/s13568-014-0016-0. (Accessed 1 April 2014).
Vilela, A., 2019. The importance of yeasts on fermentation quality and human health-promoting compounds. Fermentation 5 (2). https://doi.org/10.3390/fermentation5020046.
Wagner, A., Whitaker, R.J., Krause, D.J., Heilers, J.H., Van Wolferen, M., Van Der Does, C., Albers, S.V., 2017. Mechanisms of gene flow in archaea. Nat. Rev. Microbiol. 15 (8), 492–501. https://doi.org/10.1038/nrmicro.2017.41.
Wang, X., Kinziabulatova, L., Bortoli, M., Manickoth, A., Barilla, M.A., Huang, H., Blancafort, L., Kohler, B., Lumb, J.P., 2023. Indole-5,6-quinones display hallmark properties of eumelanin. Nat. Chem. 15 (6), 787–793. https://doi.org/10.1038/s41557-023-01175-4.
Wani, A.K., Akhtar, N., Sher, F., Navarrete, A.A., Américo-Pinheiro, J.H.P., 2022. Microbial adaptation to different environmental conditions: molecular perspective of evolved genetic and cellular systems. Arch. Microbiol. 204 (2), 1–16. https://doi.org/10.1007/s00203-022-02757-5.
Webb, R.B., Malina, M.M., 1967. Mutagenesis in Escherichia coli by visible light. Science 156 (3778), 1104–1105. https://doi.org/10.1126/science.156.3778.1104.
Zara, G., Zara, S., Pinna, C., Marceddu, S., Budroni, M., 2009. FLO11 gene length and transcriptional level affect biofilm-forming ability of wild flor strains of Saccharomyces cerevisiae. Microbiology 155 (12), 3838–3846. https://doi.org/10.1099/mic.0.028738-0.
Zwietering, M.H., Jongenburger, I., Rombouts, F.M., van 't Riet, K., 1990. Modeling of the Bacterial Growth Curve. Applied and Environmental Microbiology 56 (6), 1875–1881. https://doi.org/10.1128/aem.56.6.1875-1881.1990. https://journals.asm.org/doi/10.1128/aem.56.6.1875-1881.1990.